JES Focus Issue of Selected Papers from IMLB 2018

Electrochemical Performance of All-Solid-State Sodium-Ion Model Cells with Crystalline Na_xCoO_2 Thin-Film Cathodes

P. Kehne,[1] C. Guhl,[2] Q. Ma,[3] F. Tietz,[3,4] L. Alff,[1] R. Hausbrand,[2] and P. Komissinskiy[1]

[1]*Advanced Thin Film Technology, Institute of Materials Science, TU-Darmstadt, D-64287 Darmstadt, Germany*
[2]*Surface Science, Institute of Materials Science, TU-Darmstadt, D-64287 Darmstadt, Germany*
[3]*Forschungszentrum Jülich GmbH, Institute of Energy and Climate Research, Materials Synthesis and Processing (IEK-1), 52425 Jülich, Germany*
[4]*Helmholtz-Institute Münster, Forschungszentrum Jülich GmbH, D-52425 Jülich, Germany*

A common way to improve the electrochemical performance of the Na_xCoO_2 thin-film cathodes is to increase their crystallinity. Here we present our study of the electrochemical performance of all-solid-state sodium ion batteries with Na_xCoO_2 thin-film cathodes having two different degrees of crystallinity tuned by their post-deposition annealing at 700°C. The Na_xCoO_2 cathode thin-films were grown by pulsed laser deposition onto a bulk $Na_{3.4}Sc_{0.4}Zr_{1.6}(SiO_4)_2(PO_4)$ (Nasicon) solid electrolyte substrates and assembled with sodium metal into a Swagelok battery cells. Cells with the low-crystalline Na_xCoO_2 cathodes show discharge capacities of up to 124 mAh g^{-1} over 800 charge/discharged cycles. However, cells with highly crystalline Na_xCoO_2 cathodes revealed a significant capacity loss down to 9 mAh g^{-1} and a pronounced increase of the overpotential from 100 to 890 mV during the 200 cycles. The observed loss in capacity can be attributed to a strong increase of the interface resistance between the highly crystalline annealed Na_xCoO_2 films and Nasicon during cycling.

 [DOI: 10.1149/2.0491903jes]

Manuscript submitted October 29, 2018; revised manuscript received December 18, 2018. Published January 16, 2019. *This paper is part of the JES Focus Issue of Selected Papers from IMLB 2018.*

As model all-solid-state thin-film batteries allow good contact with a well-defined interface area between the electrode materials, they are useful to investigate correlations between the materials properties and electrochemical battery performance.[1–5] In particular, the effect of annealing of the cathode materials on their electrochemical capacity can be studied using thin-film model battery systems. "Wang et al. reported on highly crystalline thin-film $LiCoO_2$/LiPON/Li cells which showed maximum discharge rates, capacities, and cycling stability after annealing at 700°C in air. Cells with amorphous or low-crystalline (annealing at 500°C) $LiCoO_2$ cathodes exhibited initial capacity losses in the 1st charge/discharge cycle due to a loss of "available lithium sites", whereas the following decrease of the capacity was attributed to a rise of the cell resistance, especially located at the LiPON/$LiCoO_2$ interface. As the capacity fade and the interface resistance were dependent on the thickness and crystallinity of the cathode, it was speculated that the resistance increase results from strain-induced degradation of the cathode in an ill-defined region close to the electrolyte.[6]

While plenty of research was carried out on thin-film lithium ion-batteries, especially with LiPON solid electrolytes which can be sputtered at low temperatures, there are only a few studies on thin-film sodium-ion batteries.[7,8] For sodium-ion batteries, it appears to be challenging to deposit a thin-film heterostructure of phase-pure cathode, solid electrolyte, and anode due to the lack of a solid electrolyte comparable to LiPON.[9,10] A more convenient approach is to produce a thin-film all-solid state sodium battery by depositing cathode and/or anode thin-films onto a bulk solid-state electrolyte substrate.[1]

Previously we reported on polycrystalline scandium-substituted $Na_{3.4}Sc_{0.4}Zr_{1.6}(SiO_4)_2(PO_4)$ solid electrolyte of the "Na-super-ion-conductor" Nasicon-type framework (hereinafter denoted as Nasicon), which exhibited Na-ion conductivities of 4.0×10^{-3} S cm^{-1} at 25°C. Later the (de-)intercalation of sodium (from) to Na_xCoO_2 was investigated using the planar solid state batteries with 600–800 nm thick Na_xCoO_2 cathode films grown on the Nasicon substrates using Pulsed Laser Deposition (PLD) and magnetron sputtering.[11–14] Na_xCoO_2 is one of the most extensively investigated layered cathode materials for Na intercalation with a reported specific capacity of up to 107 mAh g^{-1} in the P2-phase between 2.0 and 3.8 V and good electrochemical cyclability.[15–18] Na_xCoO_2 is build up by sheets of edge sharing CoO_6 octahedra and interstitial prismatic sites into which the sodium ions are intercalated.[19–21] Occupation of these sites depends on the sodium content, resulting in phase transitions in Na_xCoO_2, which correlate with changes in the electrochemical potential of the battery cell.[22]

In this paper, we study the electrochemical performance of differently crystalline Na_xCoO_2/Nasicon/Na thin-film batteries, with Na_xCoO_2 cathode deposited at 550°C and post-annealed at 700°C. The effects of interphase formation and oxygen deficiency are evaluated by XRD, XPS, Raman and impedance measurements.

Experimental

Nasicon solid electrolyte powder with a composition of $Na_{3.4}Sc_{0.4}Zr_{1.6}(SiO_4)_2(PO_4)$ was prepared as described in Ref. 13, pressed and sintered to 1.3 mm thick discs of 10 mm in diameter.

The Nasicon disks were polished on both sides to a surface RMS roughness of 25 nm with a water-based SiO_2 polishing solution. After polishing, the disks were cleaned in water using an ultrasonic bath and later heated to 800°C for 1 hour in air to remove products of surface reactions of Nasicon with H_2O and CO_2.

Polycrystalline 700–800 nm thick Na_xCoO_2 films were deposited by PLD from a target with a Na to Co ratio of 3:1, synthesized from the powder mixtures of Na_2CO_3 (Alpha Aesar, 99.998% purity) and Co_3O_4 (Sigma-Aldrich, 99.99%).[23] The target was ablated with a KrF excimer laser beam at a wavelength of 248 nm, a fluence of 1.2 J/cm^2, and a repetition rate of 5 Hz. The films were deposited at 550°C in oxygen atmosphere at 0.01 mbar. A subsequent in-situ annealing of selected samples was carried out at 700°C in oxygen atmosphere at 400 mbar for 15 minutes. The high oxygen pressure is applied to reduce sodium losses and increase the crystal quality of the cathode thin-films.[23–26]

To carry out X-ray photoelectron spectroscopy (XPS), the samples were measured in-situ with a PHI Versaprobe 5000 spectrometer

[z]E-mail: kehne@oxide.tu-darmstadt.de

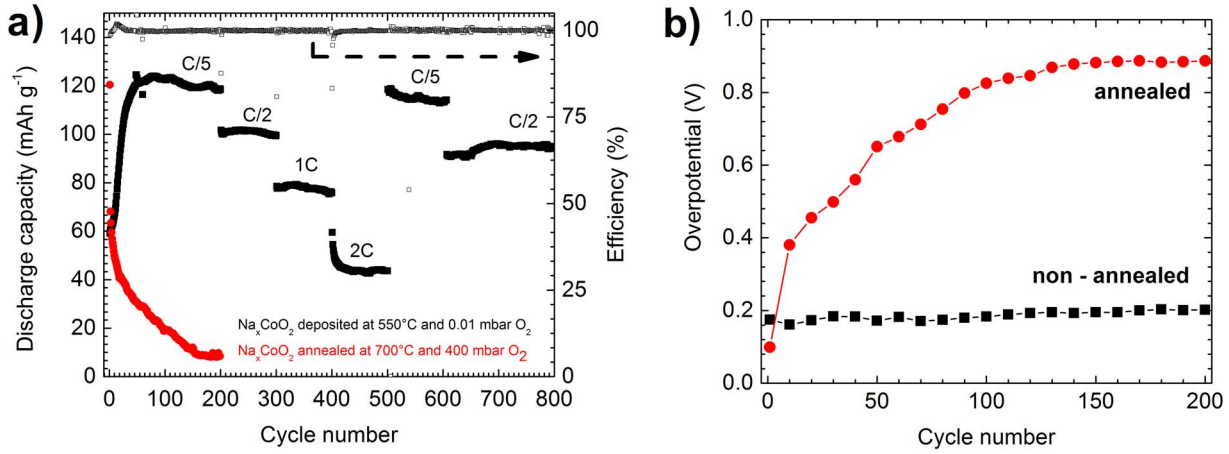

Figure 1. (a) Discharge capacities, coulombic efficiency and (b) overpotential of the Na_xCoO_2/Nasicon/Na battery with non-annealed (black) and annealed (red) cathodes.

using monochromatic Al-Kα radiation. The spectra were collected at a pass energy of 23.5 eV and an electron escape angle of 45°. The binding energies E_b were referred to the Fermi-edge position of the Ag reference sample with an uncertainty of 0.15 eV. A Shirley-type background was considered in the quantitative elemental analysis.

Produced Na_xCoO_2/Nasicon samples were assembled together with a metallic sodium anode into a Swagelok-type battery cell. The assembling was done in an Ar-filled glove box with residual concentrations of O_2 and H_2O below 0.1 ppm. Charge-discharge measurements were performed at 25°C in a climate cabinet with a VMP2 potentiometer by Bio-logic SA. The cells were cycled at current densities between 8 and 64 μA cm^{-2} in an extended voltage window from 2.0 to 4.2 V due to the higher stability of the solid electrolyte in comparison to liquid electrolytes (2.0 to 3.8 V).[14,17,27] To determine the discharge capacity of the battery, the active mass of the Na_xCoO_2 cathode was calculated by multiplying the cathode area (0.5 cm^2) with the thickness of the Na_xCoO_2 thin-film and the theoretical density of $NaCoO_2$ (5.028 g cm^{-3}).[28] All potentials are referred to the Na^+/Na couple. The overpotentials were determined from the discharge curves by evaluating the initial potential drop when the discharge current was switched on. The impedance of the Na_xCoO_2/Nasicon/Na cells was acquired at frequencies between 0.1 and 10^6 Hz at the equilibrium cell voltage of 2.68 V using a Zahner IM6 impedance analyzer.

Raman spectra were acquired in a back-scattering mode with a Horiba LabRam HR 800 micro Raman spectrometer at the excitation wavelength of 633 nm. Filtering of plasma emissions and laser-light reflection were realized with an interference filter and a Raman notch filter, respectively.

X-ray diffraction (XRD) patterns were recorded with a Rigaku Smartlab diffractometer in a parallel beam geometry using Cu-Kα radiation and a secondary graphite monochromator.

Post-mortem images of the Na_xCoO_2 films were recorded on mechanically broken Na_xCoO_2/Nasicon/Na samples with a Philips XL30 FEG scanning electron microscope (SEM) at 30 keV after electrochemical cycling. The SEM images were used for the analysis of the surface morphology of the Na_xCoO_2 films and their thickness. The latter was determined by averaging the thicknesses of the Na_xCoO_2 films measured at six cross-sectional SEM images.

Results and Discussion

Fig. 1a shows the specific discharge capacity of all-solid-state sodium ion batteries with moderately crystalline (non-annealed) and highly crystalline (annealed) Na_xCoO_2 cathodes. The initial maximum discharge capacity of the non-annealed cathode is 59 mAh g^{-1} at current densities of 8 μA cm^{-2} (C/5), and increases to a maximum value of 124 mAh g^{-1} within 100 cycles, which corresponds to 88% of the theoretical maximum discharge capacity of Na_xCoO_2 in the applied voltage range. At current densities of 16, 32 and 64 μA cm^{-2} the discharge capacity decreases to 102, 79 and 44 mAh g^{-1}, respectively, which is attributed to a large internal resistances of the battery. The battery exhibits good long-term cycling performance over 800 cycles, where the discharge capacity is reduced by 8% between the 100th and 600th cycle. In contrast, the discharge capacity of the battery with the annealed cathode faded within 200 cycles from 120 to 9 mAh g^{-1}, due to an increase of the overpotential from 100 to 890 mV, while the overpotential for the non-annealed cathode remains constant around 190 mV (Fig. 1b). An increase of the internal resistance with cycling was also observed by Wang et al., who attributed it to the cathode/solid electrolyte interface, however, this effect was predominant in amorphous or low-crystalline $LiCoO_2$ cathodes.

With electrochemical impedance measurements, the formation of an interphase between Nasicon and the annealed Na_xCoO_2 cathodes (Fig. 2a) is further supported. In agreement with other publications, the high- middle- and low -frequency half-circles can be assigned to the Nasicon solid electrolyte, the Nasicon/sodium and the Na_xCoO_2/Nasicon interface, respectively.[29–33] The initial impedance spectrum of the non-annealed cell shows accordingly a Nasicon resistance of 1.2 kΩ and a Nasicon/sodium interface resistance of 1.8 kΩ. The low-frequency half circle associated to the Na_xCoO_2/Nasicon interface is not fully evolved and, thus, difficult to evaluate. Within the first 100 cycles, the low- and medium-frequency half-circles merge and the total impedance increases to about 24 kΩ. While after the 100th cycle the total impedance of the battery with the non-annealed cathode (black) remains constant with cycling, the impedance in the annealed battery (red) drastically increases between the first and 200th cycle from 1.35 to 200 kΩ. The observation of the strong impedance increase and the fading discharge capacity within the first cycle indicates an immediate interphase formation. The impedance increase of the high-frequency half-circle, which is related to the Nasicon substrate from 1.15 to 4 kΩ, indicates a reduction of the ionic-conductivity during cycling, while it remains constant for the non-annealed sample. However, this increase in impedance is small as compared to the total impedance of 200 kΩ. The increase of the impedance up to 200 kΩ for the annealed cathode results in a calculated overpotential of 800 mV at the current of 4 μA, which is in agreement with the overpotential of 890 mV determined from the charge/discharge curves. The overpotential of 890 mV shrinks the effective potential window of the battery from 2.0–4.2 V to 2.9–3.3 V and, thus, drastically reduces the discharge capacity of the battery.

Previously Wang et al. related the increase of the internal resistance of the investigated $LiCoO_2$/LiPON/Li thin-film batteries to strain-induced changes in the cathode structure due to the intercalation and deintercalation of lithium ions, which led to large cracks in the $LiCoO_2$

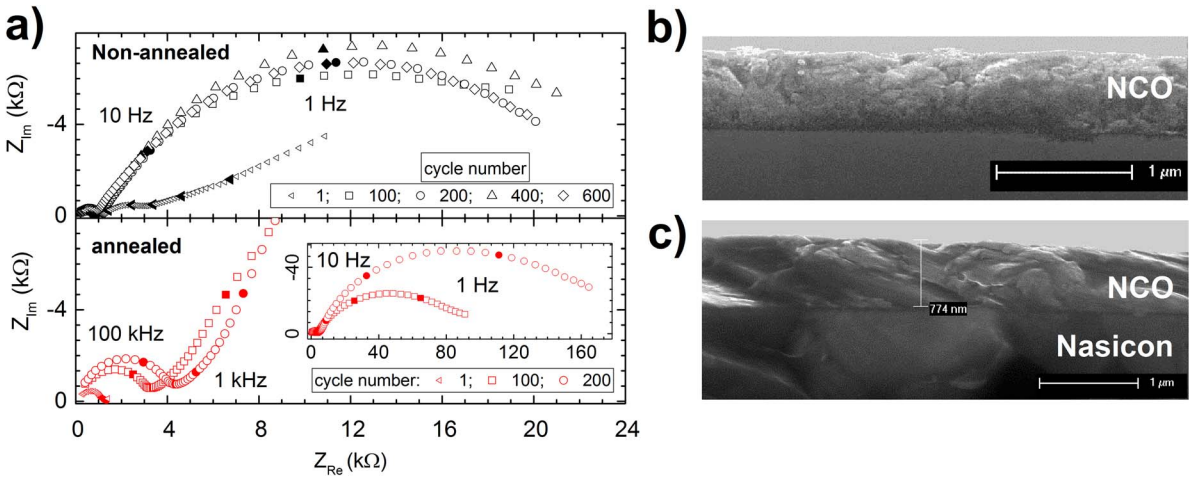

Figure 2. (a) Nyquist plots of the non-annealed (bottom panel) and annealed (top panel) Na_xCoO_2/Nasicon/Na cells after 1, 100, 200, 400, and 600 charge/discharge cycles. The high- and low-frequency half-circles are related to the Nasicon and the Na_xCoO_2/Nasicon interface, respectively. Inset. Full-scale Nyquist plot of the annealed Na_xCoO_2/Nasicon/Na cell. Cross-sectional SEM images of the Na_xCoO_2/Nasicon interfaces of the 770 nm thick (b) annealed and (c) non-annealed cathodes.

cathodes.[6] To rule out cracking or exfoliation effects between the Nasicon electrolyte and the Na_xCoO_2 thin-film cathode, cross-sectional SEM images were taken after cycling (Figs. 2b and 2c). Fig. 2b shows the microstructure of the non-annealed Na_xCoO_2 film with grain sizes smaller than 1 μm and no strain-induced cracking after cycling. The microstructure of the cathode appears to be similar to Li-ion cells which were annealed at 600°C[1] and exhibited a stable cycling performance over 100 cycles, which is in agreement with our findings. In Fig. 2c, an enhanced crystallization of the annealed Na_xCoO_2 cathodes is depicted, where the microstructure is more homogenous and no evidence of cracking is observed. Although the improved crystallinity of the annealed cathodes implies an improved ion transport, the cycling performance of the cells with the annealed Na_xCoO_2 is worse as compared to the cells with non-annealed Na_xCoO_2 due to the observed interphase formation.

To further validate the evolution of an interphase during cycling, XRD measurements on both cells with the non-annealed and annealed Na_xCoO_2 films were carried out before cycling and on the disassembled cycled cells (Fig. 3a). All peaks marked with an asterisk belong to the Nasicon substrate and remain unchanged after deposition, annealing and cycling[13] The XRD patterns of the non-annealed cathodes exhibit a low intensity (002) Na_xCoO_2 diffraction peak which consist of at least two overlapping peaks at $2\theta = 16.16°$ and 16.5°. The broad peak reflects an inhomogeneous pristine sodium distribution in the Na_xCoO_2 cathode between $0.65 < x < 0.83$.[22] During cycling, the overlapping of the peak increases, leading to a higher peak intensity, which can be interpreted as homogenization of the sodium content. Different sodium contents in neighboring Na_xCoO_2 grains are only stable if the ionic conduction between them is restricted, otherwise equilibration would take place intrinsically. We suspect an "activation" of inactive Na_xCoO_2 grains due to an improved interconnection of initially isolated particles, which explains the increasing discharge capacity during the first 100 charge/discharge cycles while maintaining a constant overpotential. (Figs. 1a and 1b). Further support for this hypothesis can be found in the impedance spectra between the first and 100th cycle, where the low frequency region, which is commonly attributed to sodium diffusion limitations is changing from an open to a full half-circle.[34]

A higher crystallinity of the annealed Na_xCoO_2 films compared to the non-annealed ones, is indicated by the high-intensity (002) and (004) peaks at $2\theta = 16.25$ and 32.75°, respectively. The peak position corresponds to a sodium content of $x = 0.71$, which is in

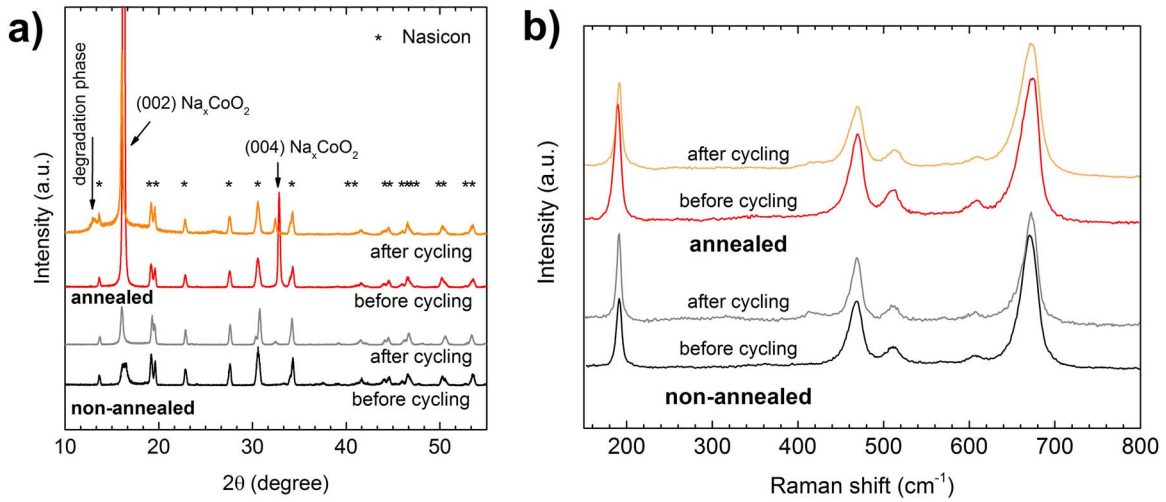

Figure 3. (a) XRD and (b) Raman spectra of the non-annealed and annealed Na_xCoO_2 cathodes on Nasicon before (black and red) and after cycling (gray and orange), respectively.

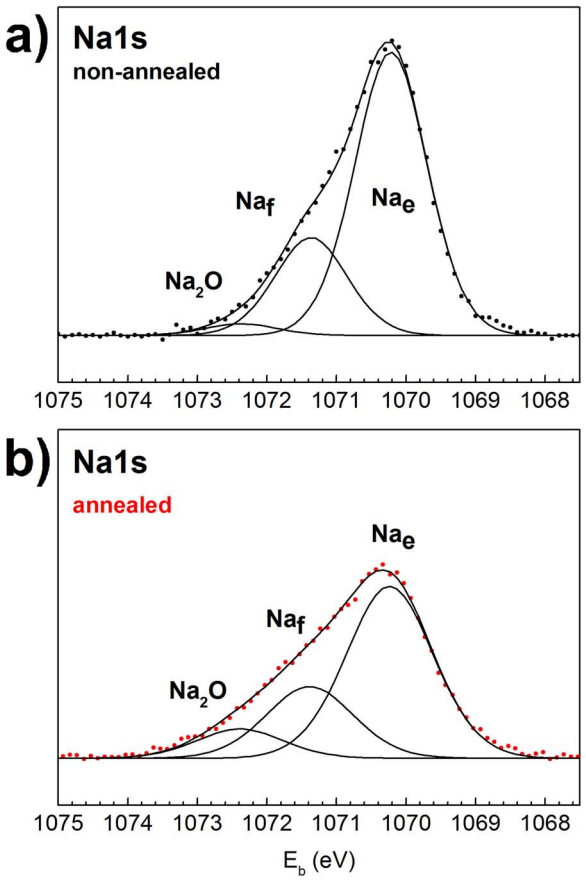

Figure 4. (a) Na1s emission of Na_xCoO_2 cathode after deposition at 0.01 mbar O_2 and (b) after annealing at 700°C in 400 mbar O_2. Peaks denoted with Na_e (edge sharing) correspond to sodium ions which are connected to six CoO_6 octahedra and Na_f (face sharing) are located directly between two CoO_6 octahedra.

good agreement with the composition of x = 0.74 obtained from XPS (Figs. 4a and 4b). However, the annealing procedure of the Na_xCoO_2 films enables the formation of a crystalline interphase associated with a diffraction peak around $2\theta = 13.0°$ during electrochemical cycling. The diffraction angle is identical to reported values of the (111) orientation of Na_4SiO_4 sodium silicate. The raised background between $2\theta = 10$ and 20° may be related to an amorphous interphase which results from a decomposition of the Nasicon substrate.

To further identify the forming interphase, Raman measurements were carried out before and after cycling (Fig. 3b). The Raman spectra of the non-annealed and annealed Na_xCoO_2 cathodes show the characteristic five Raman modes of the isomeric P2- Na_xCoO_2 phase at 191.2, 468.2, 511.1, 607.9 and 670.4 cm^{-1}.[35] Slight difference to the previously reported mode positions can be attributed to minor variations in the sodium content of the samples.[36–38] The positions of the Raman peaks before and after cycling remain unchanged, showing that the Na_xCoO_2 cathode remains intact, independent on the deposition temperature and electrochemical cycling. However, a small peak at 413 cm^{-1} arises in the Raman spectra of both cells after cycling. The peak position may be explained with a reported Raman mode of Na_4SiO_4 at 435 cm^{-1}, which would coincide with the findings by XRD. An unambiguous identification of the interphase is not possible due to the small number of peaks obtained from XRD and Raman measurements. However, the formation of an interphase at the Na_xCoO_2/Nasicon interface is strongly emphasized by the results of the electrochemical cycling and XRD measurements. The interphase causes an increase of the internal resistance of the battery and leads to the capacity fading from 120 to 9 mAh g^{-1}.

Special attention was paid to oxygen deficiency which is known from $Li_xCoO_{2-\delta}$ to have strong effects on the cycling performance. Previously, the decrease of oxygen concentration in $Na_xCoO_{2-\delta}$ from $\delta = 0.004$ to 0.073 was reported to decrease the discharge capacity of the Na_xCoO_2 cathode due to the electrons arising from the formed oxygen vacancies, which partially compensate the positive charge carriers.[39] To determine the $Na_xCoO_{2-\delta}$ thin-film stoichiometry, surface sensitive XPS measurements were carried out after the cathode film deposition and annealing without exposing the samples to atmosphere. The evaluation of the Na1s, Cop3/2 and O2s emissions results in a composition of $Na_{0.92}CoO_{1.92}$ after deposition and $Na_{0.97}CoO_{2.35}$ after annealing. The increase in sodium and oxygen amounts is explained by the formation of Na_2O at the surface due to sodium segregation.[40] Taking the Na_2O amount into account, the corrected stoichiometry of $Na_{0.86}CoO_{1.86}$ and $Na_{0.74}CoO_{2.07}$ for the non-annealed and annealed cathodes, respectively, was extracted from the analysis of the Na1s spectra in Figs. 4a and 4b. The corrected compositions are in agreement with ones obtained from the results of the XRD measurements (Fig. 3a). The measured Na1s emissions are fitted with three peaks at $E_b = 1070.2$, 1071.4, and 1072.4 eV, where the first two Na_e and Na_f peaks correspond to the edge- and face-sharing sodium sites in the Na_xCoO_2 structure,[11] respectively, and the third peak is related to Na_2O.[41] By annealing the Na_xCoO_2 cathode at 400 mbar oxygen pressure, the decreased oxygen deficiency is expected to positively influence the discharge performance of the full battery. However, even with an improved oxygen stoichiometry, the discharge capacity reduces drastically, because of the strong increase of the overpotential due to higher internal resistance of the battery (Fig. 1b), which overlays the expected positive effects.

Conclusions

The electrochemical performance of Na_xCoO_2/Nasicon/Na model batteries with a medium (non-annealed) and highly crystalline (annealed) Na_xCoO_2 cathode was investigated with a special focus on the stability of the Na_xCoO_2/Nasicon interface. Thin-film all-solid state model cells with the moderately crystalline Na_xCoO_2 cathode, $Na_{3.4}Sc_{0.4}Zr_{1.6}(SiO_4)_2(PO_4)$ solid state electrolyte, and sodium anode showed excellent cycling performance over 800 charge/discharge cycles with maximum discharge capacities of up to 124 mAh g^{-1}. Annealing the cathode at 700°C for 15 minutes produced highly-crystalline Na_xCoO_2 which, however, resulted in an exponential fading of the capacity down to 9 mAh g^{-1} after 200 cycles. The performed X-ray, Raman, and impedance measurements show that the observed capacity fading is strongly related to presumably Na_4SiO_4 interphase formation at the Na_xCoO_2/Nasicon interface. The interphase increased the observed overpotential of the cell from 100 to 870 mV and, thus, strongly reduced the observed discharge capacity. Thus, in comparison to common material systems like $LiCoO_2$/LiPON, it is not advisable to anneal the Na_xCoO_2 cathode to increase the battery performance.

Acknowledgments

This work was funded by the Deutsche Forschungsgemeinschaft (DFG) within HA 6128/2-1 and KO 4093/2-1.

ORCID

P. Kehne https://orcid.org/0000-0002-2760-8337
F. Tietz https://orcid.org/0000-0002-3724-7627
R. Hausbrand https://orcid.org/0000-0003-4601-4769
P. Komissinskiy https://orcid.org/0000-0003-1891-3011

References

1. S. Ohta, T. Kobayashi, J. Seki, and T. Asaoka, *J. of Power Sources*, **202**, 332 (2012).
2. D. Fujimoto, N. Kuwata, Y. Matsuda, J. Kawamura, and F. Kang, *Thin Solid Films*, **579**, 81 (2015).
3. J. Bates, *Solid State Ion.*, **135**(1–4), 33 (2000).

4. J. B. Bates, N. J. Dudney, G. R. Gruzalski, R. A. Zuhr, A. Choudhury, C. F. Luck, and J. D. Robertson, *J. of Power Sources*, **43**(1–3), 103 (1993).
5. N. Kuwata, J. Kawamura, K. Toribami, T. Hattori, and N. Sata, *Electrochem. Commun.*, **6**(4), 417 (2004).
6. B. Wang, *J. Electrochem. Soc.*, **143**(10), 3203 (1996).
7. M. M. Doeff, S. J. Visco, M. Yanping, M. Peng, D. Lei, and L. C. de Jonghe, *Electrochim. Acta*, **40**(13–14), 2205 (1995).
8. Q. Sun, Y. Yang, and Z.-W. Fu, *Electrochem. Commun.*, **16**(1), 22 (2012).
9. D. Horwat, J. F. Pierson, and A. Billard, *Surf. Coat. Technol.*, **201**(16–17), 7060 (2007).
10. G. Collin and J. P. Boilot, in *Superionic solids and solid electrolytes: Recent trends*, A. L. Laskar, Editor, p. 227, Boston, Acad. Pr (1989).
11. C. Guhl, P. Kehne, Q. Ma, F. Tietz, L. Alff, P. Komissinskiy, W. Jaegermann, and R. Hausbrand, *Rev. Sci. Instrum.*, **89**(7), 073104 (2018).
12. C. Guhl, P. Kehne, Q. Ma, F. Tietz, P. Komissinskiy, W. Jaegermann, and R. Hausbrand, *Electrochim. Acta*, **268**, 226 (2018).
13. Q. Ma, M. Guin, S. Naqash, C.-L. Tsai, F. Tietz, and O. Guillon, *Chem. Mater.*, **28**(13), 4821 (2016).
14. P. Kehne, C. Guhl, Q. Ma, F. Tietz, L. Alff, R. Hausbrand, and P. Komissinskiy, *Journal of Power Sources*, **409**, 86 (2019).
15. X. Xiang, K. Zhang, and J. Chen, *Adv. Mater.*, **27**(36), 5343 (2015).
16. H. Pan, Y.-S. Hu, and L. Chen, *Energy Environ. Sci.*, **6**(8), 2338 (2013).
17. J. J. Ding, Y. N. Zhou, Q. Sun, X. Q. Yu, X. Q. Yang, and Z. W. Fu, *Electrochim. Acta*, **87**, 388 (2013).
18. B. Venkata Rami Reddy and S. Gopukumar, *ECS Transactions*, **53**(30), 49 (2013).
19. A. K. Rai, L. T. Anh, J. Gim, V. Mathew, and J. Kim, *Ceram. Int.*, **40**(1), 2411 (2014).
20. D. Baster, K. Dybko, M. Szot, K. Świerczek, and J. Molenda, *Solid State Ionics*, **262**, 206 (2014).
21. T. Shibata, W. Kobayashi, and Y. Moritomo, *AIP Adv.*, **3**(3), 32104 (2013).
22. R. Berthelot, D. Carlier, and C. Delmas, *Nat. Mater.*, **10**(1), 74 (2011).
23. S. Hildebrandt, P. Komissinskiy, M. Major, W. Donner, and L. Alff, *Thin Solid Films*, **545**, 291 (2013).
24. Y. Krockenberger, I. Fritsch, G. Christiani, H.-U. Habermeier, L. Yu, C. Bernhard, B. Keimer, and L. Alff, *Appl. Phys. Lett.*, **88**(16), 162501 (2006).
25. Y. Krockenberger, I. Fritsch, G. Cristiani, A. Matveev, L. Alff, H.-U. Habermeier, and B. Keimer, *Appl. Phys. Lett.*, **86**(19), 191913 (2005).
26. L. Yu, Y. Krockenberger, I. Fritsch, and H.-U. Habermeier, *Progress in Solid State Chemistry*, **35**(2–4), 545 (2007).
27. C. Delmas, J. Braconnier, C. Fouassier, and P. Hagenmuller, *Solid State Ionics*, **3–4**, 165 (1981).
28. Y. Takahashi, Y. Gotoh, and J. Akimoto, *J. Solid State Chem.*, **172**(1), 22 (2003).
29. R. Koerver, I. Aygün, T. Leichtweiß, C. Dietrich, W. Zhang, J. O. Binder, P. Hartmann, W. G. Zeier, and J. Janek, *Chem. Mater.*, **29**(13), 5574 (2017).
30. W. Zhang, D. A. Weber, H. Weigand, T. Arlt, I. Manke, D. Schröder, R. Koerver, T. Leichtweiss, P. Hartmann, W. G. Zeier, and J. Janek, *ACS Appl. Mater. Interfaces*, **9**(21), 17835 (2017).
31. A. Sakuda, A. Hayashi, and M. Tatsumisago, *Chem. Mater.*, **22**(3), 949 (2010).
32. J. T. S. Irvine, D. C. Sinclair, and A. R. West, *Adv. Mater.*, **2**(3), 132 (1990).
33. J. P. Schmidt, T. Chrobak, M. Ender, J. Illig, D. Klotz, and E. Ivers-Tiffée, *J. Power Sources*, **196**(12), 5342 (2011).
34. H. Xia, L. Lu, and G. Ceder, *Journal of Power Sources*, **159**(2), 1422 (2006).
35. H. X. Yang, Y. Xia, Y. G. Shi, H. F. Tian, R. J. Xiao, X. Liu, Y. L. Liu, and J. Q. Li, *Phys. Rev. B*, **74**(9), 424 (2006).
36. Y. G. Shi, Y. L. Liu, H. X. Yang, C. J. Nie, R. Jin, and J. Q. Li, *Phys. Rev. B*, **70**(5), 1 (2004).
37. I. Lorite, J. J. Romero, and J. F. Fernández, *J. Raman Spectrosc.*, **43**(10), 1443 (2012).
38. J. F. Qu, W. Wang, Y. Chen, G. Li, and X. G. Li, *Phys. Rev. B*, **73**(9), 250 (2006).
39. J. Molenda, C. Delmas, P. Dordor, and A. Stoklosa, *Solid State Ionics*, **12**, 473 (1984).
40. J. P. Kemp, D. J. Beal, P. A. Cox, and J. S. Foord, *Vacuum*, **41**(7–9), 1739 (1990).
41. A. Barrie and F. J. Street, *J. Electron. Spectrosc. Relat. Phenom.*, **7**(1), 1 (1975).